Drought response of tree-ring width in the southern boundary of Pinus tabulaeformis from Mt. Funiu, central China

Jianfeng Peng (jfpeng@vip.henu.edu.cn)
Henan University
Jinbao Li
University of Hong Kong
Xuan Li
Henan University
Jiayue Cui
Henan University
Meng Peng
Henan University

Research Article

Keywords: tree-ring, Pinus tabulaeformis Carr., drought variation, transition zone, central China

Posted Date: March 24th, 2022

DOI: https://doi.org/10.21203/rs.3.rs-1448882/v1

Abstract

Tree ring data from the southern boundary of *Pinus tabulaeformis* distribution where is the southern margin of warm temperate, the paper analyzes the response of climate factors along north-south direction to tree growth. The results show that temperature and precipitation in May-June and relative moisture from March to June are main limiting factors on tree growth; however, the temperature in the south of the mountain and the humidity in the north of the mountain have relatively greater influence on tree growth. The regional $scPDSI_{MJ}$ (that is PDSI in May-June) is the most significant and stable limiting factors on tree growth to be used for reconstruction, which explains 50.4% of the variance in the instrumental records from 1963 to 2016 CE. The reconstructed $scPDSI_{MJ}$ revealed that there were 29 extremely dry years (accounting for 12.96%) and 30 extremely wet years (accounting for 13.89%) and it can represent the drought variation in central and eastern monsoon region, and agree with the reconstructed PDSI for Mt. Shennong and the drought/wetness series in Zhengzhou, with correlation coefficients 0.367 (n = 210, $p = 0.000$) and 0.196 (n = 200, $p = 0.005$), respectively. Further research found that drought of May-June in central China mainly impacted by local temperature and moisture (including precipitation, soil moisture, potential evaporation and water pressure), and then the Pacific and the Atlantic. These results may provide better understanding of May-June drought variation and service for agricultural production in central China.

1. Introduction

Under global warming, the frequency and intensity of extreme weather events are likely to increase dramatically, which will have a more serious impact on ecosystems and human society and require more timely and effective responses (IPCC, 2014). The typical continental monsoon climate in the middle and lower reaches of the Yellow River can cause the instability and variability of the climate due to the changes of monsoon strength and the early and late of monsoon rains. These changes may be result in frequent flood and drought in the region and directly related to the harvest of agricultural years. Hence the climate changes in the future may not only affect living environment and ecological security, also put forward severe challenges to the high quality and sustainable development of the middle and lower reaches of the Yellow River region.

There is a long history and abundant climatic records in the middle and lower reaches of the Yellow River, and also has some reconstructed drought-flood information based on historical documents but often non-quantitative and discontinuous. Dendroclimatology is a science that reconstructs past climate changes based on tree physiology and tree radial growth characteristics (Fritts,1976;Wu, 1990). Tree-ring data have the advantages of high resolution (annual or seasonal) and precise-continuous series for dating, and it has been successfully used to quantitatively characterize the climate change series and regarded as one of the most important proxy indicators in the past climate change research (Fritts,1976; Cook et al, 2010).

In recent years, dendrochronological studies in eastern China had been developing rapidly (Cai et al, 2013, 2018;Cheng et al, 2012, 2015, 2021; Duan et al, 2012Fang et al, 2017Peng et al, 2014, 2018, 2019, 2020; Shi et al, 2013, 2017; Zhang et al, 2017; Zhao et al, 2019Zheng et al, 2012, 2016). However, dendrochronological study is still limited in Mt. Funiu of western Henan Province as a climatic transition zone (Tian et al, 2009Shi et al, 2012Liu et al, 2015, 2017Zhao et al, 2019Peng et al, 2020; Yang et al, 2021). There are some hydroclimate reconstructions in Mt. Funiu, e.g., temperature (Shi et al, 2009Tian et al, 2009Liu et al, 2014, 2015Yang et al, 2021), relative humidity (Liu et al, 2017Peng et al, 2020), scPDSI (Zhao et al, 2019). To some extent, the above studies are helpful to understand climate change in Mt. Funiu and its surrounding areas. To better reveal the impact and formation mechanism on climate change and more understood climate change affecting ecological security and high-quality development in central Plains, further study of tree rings in Mt. Funiu is necessary.

This study was mainly used to compare correlation between tree-ring data and north-south climatic factors (including scPDSI grid data) in Mt. Funiu and the transitional characteristics of performance; Secondly the most significant climate limiting factors were selected to carry out climate reconstruction and analysis it's spatial representations, and finally further to explore the possibility and potential impact of future climate change in this region.

2. Data And Methods

2.1 Study area

Mt. Shiren (33º43'39.49"N, 112º15'4.39"E, 1775 m a.s.l.) is located in western Henan province in central eastern Qinling Mountains, central China (Fig. 1). It is a transitional zone from subtropical to warm temperate continental monsoon climate with mildly wet summers and cold dry winters. It is also the transition zone from humid to sub-humid. The annual mean temperature is 10.0°C and annual amount of precipitation is 820–860 mm, and mean temperature in January is -3.3°C while July is 20.3°C. The forests canopy cover is about 95%, the dominant vegetation is the mixed forests composed of temperate deciduous broad-leaved and coniferous on the top of the mountain, including *P. tabulaeformis* carr. and *P. armandi* Franch LC. The soil is typically brown mountain soil with 30 to 40 cm deep. The species for our study, *P. tabulaeformis Carr.*, is mainly distributed between 1300 m and 1800 m a.s.l. The species is very sensitive to climate change because the eastern Mt. Funiu is the southern boundary of the Chinese Pine distribution (Xu,1993).

2.2 Chronology and climate data

Tree-ring data of *P. tabulaeformis* Carr is from Mt. Shiren in western Henan province which had been studied tree growth response to east-west climate factors (from Luanchuan and Baofeng meteorological stations) in previous studies (Peng et al., 2020; Yang et al., 2021). The sampling site is in central eastern Mt. Funiu, central China. The reliable standard chronology from 1801 to 2016 CE, with the starting year determined by adopting a sub-sample signal strength (SSS) threshold of 0.85 (Wigley et al. 1984), was

developed and used. The chronology contains high signal-to-noise ratio (SNR, 14.543) and the expressed population signal (EPS, 0.936), so it demonstrated a high level of reliability.

To better understand transitional characteristics of tree growth in Mt.Funiu, the study selected Songxian meteorological station of northern Mt. Funiu and Neixiang meteorological station of southern Mt. Funiu (Fig. 1, Table 1) along the gradient of temperature and precipitation in the north and south (that is along gradient from warm temperate to subtropical monsoon climate). Climate factors used in this study include monthly mean temperature (T), monthly mean maximum temperature (Tmax), monthly mean minimum temperature (Tmin), monthly total precipitation (P), and monthly mean relative humidity (RH) during 1963–2016 (Fig. 2).

The self-calibrating Palmer Drought Severity Index (scPDSI, van der Schrier et al., 2013) was chosen as a metric to measure the responses of tree growth to moisture conditions. The four grids and a regional mean of the scPDSIs between 33.5 to 34.5N and 111.5 to 112.5E (CRU scPDSI 3.26e, https://climexp.knmi.nl/; Fig. 1, Table 1) were also used in this study, respectively.

Table 1
Characteristics of climate data used in correlation analyses

Climate data Source	Latitude(°N)	Longitude(°E)	Elevation (m a.s.l.)	Time Spaning
Songxian	34.13	112.06	440.7	1963–2016
Neixiang	33.15	111.88	221.4	1963–2016
scPDSI-1	33.75	111.75	-	1963–2016
scPDSI-2	33.75	112.25	-	1963–2016
scPDSI-3	34.25	111.75	-	1963–2016
scPDSI-4	34.25	112.25	-	1963–2016
Regional scPDSI	33.5–34.5	111.5-112.5	-	1963–2016

2.3 Statistical methods

Pearson's correlation analyses were performed to identify climate-growth relationships between tree-ring standard chronology and climatic factors from two meteorological stations. Climate-growth relationships were investigated from previous March to current November to explore the potential effects of climatic factors on trees growth from the previous year to the current year.

Then, a simple linear regression model based on the most dominant climatic factor was selected and reconstructed. The split calibration-verification procedure was used to verify the reconstruction (Cook et al., 1999), statistical parameters for this assessment include correlation coefficient (r), R-squared (R^2),

sign test (ST), reduction of error (RE), and coefficient of efficiency (CE). In general, positive RE and CE indicate a rigorous and reliable reconstruction model (Cook et al. 1999).

Spectral analyses were performed using Multi-Taper Method (MTM) (Mann and Lee 1996) to detect the periodicities of the reconstruction, and Wavelet analysis (Torrence and Compo, 1998) was used to extract strong or weak changes for different cycle signals in the reconstruction.

Spatial analyses were performed between the reconstructed $scPDSI_{MJ}$ and scPDSI (1963–2016; 4.05early), temperature, precipitation, potential evaporation, vapor pressure (1963–2016; CRU TS4.04) and soil moisture (1979–2016; CLM/EARi, 0-10cm) (references for European Climate Assessment & Data) to explore regional representation and possible formation mechanisms. The analyses were performed on the KNMI Climate Explorer (http://climexp.knmi.nl).

3. Results

3.1. Climate-growth relationship

There are significant negative correlations ($p < 0.05$) with T, Tmax and Tmin in current May and June (Fig. 3), and also significant negative correlations with Tmax in current March and April. There are similar significantly negative correlations with temperatures from two meteorological stations, which indicated the strong effect of temperature on tree growth and the influence time of Tmax to tree growth is longer. In contrast, the chronology shows mostly positive correlations with P in April-May and RH in March-June at both stations. There are also significant positive correlations between chronology and current June P in Songxian station and current July RH from the Neixiang station. Overall, temperature (T, Tmax) of southern meteorological station of Mt. Shiren showed higher correlation with tree growth while the greatest influence of humidity (P, RH) were found from northern meteorological station of Mt. Shiren.

The correlations between chronology and scPDSI from previous March to current November are almost all positive, especially significant from current March to August. Almost all correlations between chronology and scPDSI in May and June are over 0.6 ($p < 0.05$), the highest correlation in May is scPDSI grid point (0.687, $p < 0.05$; 33.75N, 112.25E) closest to the sampling site while the highest correlation in June is regional mean scPDSI (0.663, $p < 0.05$; 33.5-34.5N, 111.5-112.5E).

In a general way, seasonal climate is more stable and meaningful than single month climate to tree growth. Based on the principle that a higher correlation indicates a greater impact on tree growth, we combine the monthly data on single scPDSI grid point (33.75N, 112.25E) closest to the sampling site and regional mean scPDSI (33.5-34.5N, 111.5-112.5E). The highest correlations with chronology were both May-June scPDSI, and the highest correlation value of single grid scPDSI was 0.693 ($p < 0.05$, 33.75N, 112.25E) while that of regional mean scPDSI was 0.71 ($p < 0.05$). Thus, the standard chronology of *P. tabulaeformis* Carr could be used to reconstruct regional $scPDSI_{MJ}$.

3.2 Transfer function and regional scPDSI reconstruction

According to the above correlation resultss, the regional mean scPDSI in current May-June ($scPDSI_{MJ}$) was reconstructed using following linear regression equation based on the least square method:

$scPDSI_{MJ} = 5.514*Wt - 5.21$

($N = 54$, $r = 0.71$, $R^2 = 50.4\%$, $R^2_{adj} = 49.4\%$, $F = 52.795$, $p < 0.0001$)

Where, Wt is the index of tree-ring chronology for year t.

The reconstructed $scPDSI_{MJ}$ could explain 50.4% of the variance in the instrumental record and 49.4% after an adjustment for the loss of the degree of freedom. A visual comparison also showed that the reconstructed mean $scPDSI_{MJ}$ tracked the observed $scPDSI_{MJ}$ well (Fig. 4a). The first-order difference data show that there was a significant correlation ($r = 0.737$, $p < 0.001$) between the two $scPDSI_{MJ}$ sequences (Fig. 4b), indicating that the reconstructed $scPDSI_{MJ}$ captured variations of the observed $scPDSI_{MJ}$ at both high and low frequencies.

The split sample procedure was used to assess the reliability of the reconstruction. Table 2 shows that all parameters used for calibration and verification periods are significant ($p < 0.01$) and RE and CE values are positive, and ST test is also significant ($p < 0.05$) and high F values are in all calibration and verification time periods, which means the model is acceptable for $scPDSI_{MJ}$ reconstruction (Cook et al.1999).

Table 2
Calibration and verification statistics for reconstructed $scPDSI_{MJ}$

	Calibration (1963–1991)	Verification (1992–2016)	Calibration (1988–2016)	Verification (1963–1987)	Full calibration (1963–2016)
R	0.714**	0.696**	0.814**	0.601**	0.710**
R^2	0.510	0.485	0.662	0.361	0.504
CE		0.298		0.324	
RE		0.668		0.440	
ST	22+/7–**	18+/7–*	22+/7–**	19+/6–*	41 + 13–**
F	28.108	21.663	52.948	12.994	52.795
**Significant at the 99% confidence levels, *Significant at the 95% confidence levels.					

Spectral analysis results (Fig. 5) revealed that the $scPDSI_{MJ}$ reconstruction contained 2.3a, 2.86-2.9a, 3.35a, 3.69-3.83a and 6.43a cycles ($p < 0.5$), indicating potential ENSO (2-7a, El Niño-Southern Oscillation) impacts (Allan et al. 1996; Sun and Wang, 2007). There are also 34.11a, 49.26a cycles ($p <$

0.01), which may be related to PDO (Pacific Decadal Oscillation) or AMO (Atlantic Multi-decadal Oscillation) (d'Orgeville et al, 2007; Yang et al, 2017).

4. Discussion

4.1 Tree growth influenced by temperature, precipitation, or scPDSI

Previous studies demonstrated that the maximum temperature (Yang et al, 2021) and Relative Humidity (Peng et al, 2020) from April to July were main limiting factors at Mt. Shiren. Early summer moisture signals (scPDSI) were also captured and reconstructed in the eastern Mt. Qinling (Zhao et al, 2019). However, tree growth is the result of the interaction of temperature and precipitation, and temperature often affects tree growth through its effects on water availability. So temperature-raised water deficiency induces water stress to suppress cell division and expansion (Fritts, 1976) and form narrow ring.

The sampling site located in the eastern Mt. Funiu, the eastern extension of the Mt. Qinling, here is a climatic transitional belt from subtropical to warm-temperate continental monsoon. There are higher temperature and more precipitation in the subtropical zone of the southern Mt. Funiu, belong to humid climate region, while belong to sub-humid climate region in warm temperate zone of northern Mt. Funiu, so tree growths exist different response to climate in north and south Mt. Funiu. The correlation results found that tree growth in higher altitude responds similarly to climate factors on the north and south meteorological stations as described above, these are temperature and precipitation in May and June are mainly limiting factors. However, also some different response in horizontal scale which temperature (T, Tmax) of southern meteorological station (Neixiang) of Mt. Shiren had greater influence on tree growth while the greatest influence humidity (P, RH) were from northern meteorological station (Songxian).

To better understand the interaction between temperature and humidity, scPDSI was used for further research. We chose 4 single grid-points and 1□1 grid-point (33.5-34.5N, 111.5-112.5E) regional mean scPDSI near sampling site as examples to conduct correlation analyses, and found that the correlation results were consistent, with significant positively correlations from current March to August. The regional mean grid-point (33.5-34.5N, 111.5-112.5E) scPDSI contains both the sampling point and the Songxian meteorological station, and there is a good correspondence between the response of tree growth to scPDSI and the response to the precipitation of the Songxian meteorological station. This also proved that the tree growths in sub-humid areas were mainly restricted by moisture. But the highest correlation with chronology was regional mean scPDSI ($r = 0.71$, $p < 0.05$) in current May-June, while be 0.675 ($p = 0.000$) with relation humidity and 0.583 ($p = 0.000$) with precipitation in current May-June. In other words, with temperatures rising in May-June, deficiency of soil moisture limits tree growth and produce narrow rings due to a lack of precipitation before the rainy season and a high evapotranspiration rate. However, the scPDSI as a comprehensive drought index well represents the joint effects of regional temperature, precipitation and soil moisture, so scPDSI may better reflect moisture variation.

The moving correlation result shows that regional mean $scPDSI_{MJ}$ (Fig. 6) is the most significant and stable, hence it could be used for reconstruction.

4.2 Drought variation of the reconstructed $scPDSI_{MJ}$

Table 3
Moderately to extreme drought/wet events derived from tree-ring reconstructions and the corresponding descriptions of historical records.

	$scPDSI_{MJ}$ (1801–2016, this study)	RH_{AJ} (1801–2016, Peng, 2020)	$scPDSI_{MJJ}$ (1868–2005, Zhao, 2019)	Historical records in Henan Province (CCMDC,2006)
Extremely dry period	1801–1802	1801–1802	**1879**	Not available
	1807,1810	1807–1810	**1900**	Drought from spring to summer
	1813–1814	1813–1814	1923,1926,	Drought from spring to summer in 1813 and spring drought in 1814
	1835	1821	**1929**	Severe drought from spring to summer
	1847	1835–1836	1994,1995	Drought from spring to summer
	1867	1847	**2000**	Drought from spring to summer in Gongyi, Henan
	1879–1881	1867		A mega-drought caused a great famine over Henan and Shaanxi so on provinces in northern China in during 1876–1879
	1891–1892	**1879**–1881		Not available
	1900	1891–1892		Severe drought from spring to autumn over Henan and Shaanxi
	1907	**1900**		Drought from spring to summer
	1929	1907		Severe drought from spring to autumn over Henan, the river and pond dry up
	1932	**1929**		Drought from summer to autumn over Henan
	1935	1932		Severe spring drought over Henan
	1941	1935		Severe drought from spring to autumn in 1941and 1942
	1945	1941		Severe drought and locust disaster over Henan
	1955	1945		Severe drought from spring to early summer
	1968	1955		Drought from spring to summer in the most of Henan
	1988	1968,		Severe drought following the drought of 1985–1987
	1992,	1988		Severe spring drought
	2000–2001	1992,		
	2011	**2000**–2001		
		2007		

	$scPDSI_{MJ}$ (1801–2016, this study)	2011 RH_{AJ} (1801–2016, Peng, 2020)	$scPDSI_{MJJ}$ (1868–2005, Zhao, 2019)	Historical records in Henan Province (CCMDC,2006)
				Severe drought from February to May (the worst one since 1950) Severe drought from January to February since October 2010 (the lowest for the same period since 1951)

	$scPDSI_{MJ}$ (1801–2016, this study)	RH_{AJ} (1801–2016, Peng, 2020)	$scPDSI_{MJJ}$ (1868–2005, Zhao, 2019)	Historical records in Henan Province (CCMDC,2006)
Extremely wet period	1831		**1869**	Spring and summer rains from north to south of the Yellow River
	1840		1883	Not available
	1862–1864		**1885**	Not available
	1866		**1894**	Flood in March in Yexian
	1868–1872		1895	Flood in summer and autumn over Henan in 1869
	1875		**1898**	Not available
	1885		**1905**	Flood in summer in Lingbao and Shanxian (northwestern Henan)
	1894		1906	Not available
	1898		**1910–1912**	Severe flood in summer at Yi and Luo river (Henan), Shangnan (Shaanxi)
	1901		1933,1934, 1936,1944	Flood in Fangcheng (Henan)
	1905		1948,1949	Severe flood in spring and summer over Henan
	1911–1913		1973,1980, **1983**	Persistent flood in summer and autumn over Henan during 1910–1913
	1915		**1984**	Flood in summer and autumn over Henan
	1946		**1990**	Persistent rainfall in spring and summer in the most of Henan
	1950			Not available
	1983			Rainstorm in April and May in the north Henan in 1983
	1984			From June to September, there were 5 large-scale rainstorms over Henan in 1984
	1990			Not available
	1991			Rainstorm in September in Nanzhao (Henan)
	1998, 2010			Not available
				Low temperature and rain in spring, heavy rain in summer

	$scPDSI_{MJ}$ (1801–2016, this study)	RH_{AJ} (1801–2016, Peng, 2020)	$scPDSI_{MJJ}$ (1868–2005, Zhao, 2019)	Historical records in Henan Province (CCMDC,2006)
The five driest years	**1880 (-2.999)**	**1880 (57.82%)**	**1879(-3.61)**	Ding-Wu disaster, Shanxi and Henan famine, extreme drought
	1835 (-2.795)	1835 (60.05%)	2000(-2.94)	
	1955 (-2.723)	1955 (60.24%)	**1929(-2.53)**	
	1929 (-2.629)	**1929 (60.50%)**	1926(-2.33)	
	1907 (-2.552)	1907 (60.71%)	1923(-2.28)	

4.3 The spatial representations of reconstructed $scPDSI_{MJ}$

Spatial correlation analyses of actual or reconstructed regional mean $scPDSI_{MJ}$ with scPDSI (1963–2016; scPDSI, 4.05early), temperature, precipitation, potential evaporation, vapor pressure (1963–2016; CRU TS4.04) and soil moisture (1979–2016; CLM/EARi, 0-10cm) were performed to determine the spatial distribution and explore possible causes of drought/wet variations.

4.3.1 Spatial representations

Figure 8 demonstrates that the actual and reconstructed regional $scPDSI_{MJ}$ are significant positive correlations with scPDSI (1963–2016; scPDSI, 4.05early) around the study area. Obviously, the reconstructed $scPDSI_{MJ}$ may represent the drought/wetness variation in central and eastern monsoon region, especially in central China region and south adjacent area. These regions are the main grain producing areas in China, so it is very important to research drought/wet variation for grain production security in China.

In order to verify the reliability of regional representation, we compared reconstructed $scPDSI_{MJ}$ with the reconstructed PDSI of Mt. Shennong (SNPDSI, Fig. 1) and drought/wetness index from Zhengzhou (DWZZ, CMA 1981; Fig. 1 Zhengzhou). The results found that the severe drought events showed better consistency, and correlation coefficients are 0.367 (n = 210, $p = 0.000$) between $scPDSI_{MJ}$ and SNPDSI, 0.196 (n = 200, $p = 0.005$) between $scPDSI_{MJ}$ and DWZZ, and 0.190 (n = 200, $p = 0.007$) between SNPDSI and DWZZ (Fig. 9). These statistically validated the reliability and spatial representation of the reconstructed $scPDSI_{MJ}$.

The gray bars represent the same drought periods in three series.

4.3.2 Causes analysis of drought variations

The drought variation of a region is closely related to regional climatic elements. The spatial correlation results show significant negative correlations with temperature and potential evaporation and significant positive correlations with precipitation and vapor pressure and soil moisture in central China region and south adjacent region (e.g., Huanghuai region and the central-western Jianghuai region) (Fig. 10a-j), however the scale is slightly different. In terms of the perspective of affected area, temperature and soil moisture on north and south sides of the sampling site (Mt. Shiren) have similar influence on tree growth (Fig. 10, a-b and i-j), while precipitation, potential evaporation and water pressure from the north of mountains have more influence than the south of mountains (Fig. 10, c-d, e-f and g-h). These also show that drought of central China in May-June is probably mainly impacted by local temperature and moisture (including precipitation, soil moisture, potential evaporation and water pressure) on both sides of the transition zone.

4.4 The global hydro-climatic signals in reconstructed mean $scPDSI_{MJ}$

Based on the significant characteristics of monsoon climate in eastern China, this study continues to discuss the relationship between tree growth at sampling sites and global sea surface temperature (SST, NASA MERRA-2 Tsfc, 1980–2016; The relationship between tree growth and land surface temperature has been analyzed in Fig. 10a-b). Figure 11 shows there are some significant negative correlations with SST from the northern Pacific Ocean and the northern Atlantic Ocean and significant positive correlation with SST from the southeastern Pacific Ocean and the northeastern Indian Ocean with reconstructed $scPDSI_{MJ}$ in this study, but the overall correlation is weak. These results also confirm that the periodic changes (2.3-6.43a ENSO cycles ($p < 0.5$); 34.11 and 49.26 PDO or AMO cycles ($p < 0.01$)) of tree growth in the transition zone could be related to the SST changes in the Pacific and Atlantic Oceans. The conclusion, which the drought from May to June had a certain relationship with SST from the northwestern Pacific Ocean (that is PDO cycle), was similar to previous studies (Ma, 2007; Zheng et al, 2014), and same as spectral analysis previously. Example, the monsoon from the Pacific Ocean usually arrives at the middle and lower reaches of the Yangtze River in June, and the monsoon rainy season begins in the study area in late July, so the study area in May-June is a period of low rainfall. The high temperature of the northwestern Pacific Ocean surface in May-June reduces the thrust of the monsoon, making it difficult for water vapor to reach the northern China, while heat and evaporation on land lead to water shortages for limiting tree growth (Fig. 10a-b) and forming narrow ring. The spatial correlations from Fig. 11 also show that local continental temperature influence (above 0.6) is higher than that of the Pacific Ocean surface temperature (from 0.3 to 0.5), this also indicates that sea surface temperature changes in the Pacific Ocean had a greater impact on tree growth in the study area, but the impact is weaker than that on land in May and June.

5. Conclusion

Based on sampling site located in an ecological sensitive area from north subtropical to warm temperate climatic transition zone, the correlation analysis between tree-ring chronology and north-south

longitudinal meteorological data was conducted. The results found that temperature and precipitation in May-June and relative humidity from March to June are main limiting factors; however, the temperature in the south of the mountain and the moisture (including precipitation and relative humidity) in the north of the mountain had greater influence to tree growth.

The regional $scPDSI_{MJ}$ is the most significant (0.71, $p < 0.05$) and stable to be used for reconstruction, which explains 50.4% (49.4% after adjustment of the degree of freedom) of the variance in the instrumental records from 1963 to 2016 CE. The reconstructed $scPDSI_{MJ}$ revealed that there are 29 extremely dry years (accounting for 12.96%) and 30 extremely wet years (accounting for 13.89%). The five driest years were 1880 (-2.999), 1835 (-2.795), 1955 (-2.723), 1929 (-2.629) and 1907 (-2.552) over the reconstruction period. The reconstructed $scPDSI_{MJ}$ can represent the drought variation in central and eastern monsoon region and agree with the reconstructed PDSI for Mt. Shennong and the drought/wet series in Zhengzhou which correlation coefficients are 0.367 (n = 210, $p = 0.000$) and 0.196 (n = 200, $p = 0.005$), respectively.

Further research found that drought of central China in May-June was mainly impacted by local temperature and moisture (including precipitation, soil moisture, and potential evaporation and water pressure) on both sides of the transition zone, and the second one is by the Pacific and the Atlantic. These results may provide better understanding of May-June drought variation and service for agricultural production in central China.

Declarations

Acknowledgements: The authors thank Kexian Li and Lei Zhao from Mt. Shiren National Nature Reserve Bureau and Liang Chen, Kunyu Peng, and Jinrui Dan for their help during field work. The authors also thank the National Field Scientific Observation and Research Station of Forest Ecosystem in Dabie Mountains, Henan Province.

Funding: This research was funded by National Natural Science Foundation of China (No. 41671042; 42077417).

Author Contributions: JFP and JBL conceived and designed the original study. JFP, XL, MP performed statistical analyses. XL, JYC, MP, JKL and XXW interpreted the data. JFP wrote original manuscript. JBL critically revised manuscript.

Declaration of interests: The authors declare that they have no known competing financial interests or personal relationships that could have appeared to influence the work reported in this paper.

References

1. Allan RJ, Lindesay JA, Parker DE (1996) El Nino Southern Oscillation and Climatic Variability. CSIRO, Collingwood, Victoria

2. Cai QF, Liu Y (2013) The June–September maximum mean temperature reconstruction from Masson pine (*Pinus massoniana* Lamb.) tree rings in Macheng, southeast China since 1879 AD. China Science Bulletin 58(Suppl.I): 169–177(in Chinese)
3. Cai QF, Liu Y, Duan BC, Sun CF (2018) Regional difference of the start time of the recent warming in Eastern China: prompted by a 165-year temperature record deduced from tree rings in the Dabie Mountains. Climate Dynamics 50(5–6): 2157–2168
4. Chen F, Yuan YJ, Wei WS, Yu SL, Zhang TW (2012) Reconstructed temperature for Yong'an, Fujian, Southeast China: Linkages to the Pacific Ocean climate variability. Global and Planetary Change 86–87: 11–19
5. Chen F, Zhang RB, Wang HQ, Qin L (2015) Recent climate warming of central China reflected by temperature sensitive tree growth in the eastern Qinling mountains and its linkages to the Pacific and Atlantic Oceans. Journal of Mountain Science, 12(2): 396–403
6. Chen F, Gagen MH, Zhang HL, Chen YP, Fan ZA, Chen FH (2021) Warm season temperature in the Qinling Mountains (north-central China) since 1740 CE recorded by tree-ring maximum latewood density of Shensi fir. Climate Dynamics, DOI: 10.1007/S00382-021-05827-4
7. CMA (Chinese Meteorological Administration) (1981) Yearly charts of dryness/wetness in China for the last 500-year period. Cartographic Publishing House, Beijing (in Chinese)
8. Cook ER, Meko DM, Stahle DW, Cleaveland MK (1999) Drought reconstructions for the continental United States. Journal of Climate 12:1145–1162
9. Cook ER, Anchukaitis KJ, Buckley BM, D'Arrigo RD, Jacoby GC, Wright WE (2010) Asian monsoon failure and mega drought during the last millennium. Science 328:486–489.
10. Daniels, Lori (2020). What tree rings can tell us. Science 368(6488): 250
11. d'Orgeville M, Hua B L, Sasaki H (2007) Equatorial deep jets triggered by a large vertical scale variability within the western boundary layer. Journal of marine research 65: 1–25
12. Duan JP, Zhang QB, Lv LX, Zhang C (2012) Regional-scale winter-spring temperature variability and chilling damage dynamics over the past two centuries in southeastern china. Climate Dynamics 39(3–4): 919–928
13. Fang KY, Cai BG, Liu XM, Lei GL, Jiang XY, Zhao Y, Li HC, Heikki Seppä (2017) Climate of the late pleistocene and early holocene in coastal south china inferred from submerged wood samples. Quaternary International 447(aug.15): 111–117
14. Fritts HC (1976) Tree Rings and Climate. Academic Press, New York
15. IPCC (2014) Climate Change 2014: Impacts, Adaptation, and Vulnerability. Contribution of Working Grouper to the Fifth Assessment Report of the Intergovernmental Panel on Climate Change [M]. Cambridge: Cambridge University Press 1–1132
16. Liu Y, Liu H, Song HM, Li Q, George SB, Wang L, Hu SL (2017) A 174-year Asian summer monsoon related relative humidity record from tree-ring $\delta^{18}O$ in the Yaoshan region, eastern central China. Science of Total Environment 593/594: 523–534

17. Liu Y, Zhang YH, Cai QF, Song HM, Ma YY, Mei RC (2015) The tree-ring width based seasonal minimum temperature reconstruction at Shiren Mountains, Henan, China since 1850 AD and its record of 20th century warming. Journal of Earth Environment 6(6): 393–406
18. Liu Y, Zhang YH, Song HM, Ma YY, Cai QF, Wang YC (2014) Tree-ring reconstruction of seasonal mean minimum temperature at Mt. Yaoshan, China, since 1873 and its relevance to 20th-century warming. Climate of the Past Discussions 10: 859–894
19. Ma ZG (2007) Relationship between the trend of aridity in North China and the Decadal Oscillation of the Pacific Ocean. China Science Bulletin 55: 1199–1206 (in Chinese)
20. Mann ME, Lees JM (1996) Robust estimation of background noise and signal detection in climatic time series. Climatic Change 33: 409–445
21. Peng JF, Li JB, Wang T, Huo JX, Yang L (2019) Effect of altitude on climate-growth relationships of chinese white pine (*Pinus armandii*) in the northern Funiu mountain, central China. Climatic Change 154: 273–288
22. Peng JF, Li JB, Yang L, Li JR, Huo JX (2020) A 216-year tree-ring reconstruction of April-July relative humidity from Mt. Shiren, central China. International Journal of Climatology 40: 6055–6066
23. Peng JF, Liu YZ, Wang T (2014) A tree-ring record of 1920's-1940's droughts and mechanism analyses in Henan Province. Acta Ecologica Sinica 34(13): 3509–3518 (in Chinese)
24. Peng JF, Peng KY, Li JB (2018) Climate-growth response of Chinese white pine (*Pinus armandii*) at different age groups in the Baiyunshan National Nature Reserve, central China. Dendrochronologia 49: 102–109
25. Shi JF, Cook ER, Li JB, Lu, HY (2013) Unprecedented January-July warming recorded in a 178-year tree-ring width chronology in the Dabie mountains, southeastern China. Palaeogeography Palaeoclimatology Palaeoecology 381–382(7): 92–97
26. Shi JF, Li JB, David D, Zheng JY, Shi SY, Ge QS, Harry F. Lee, Zhao YS, Zhang J, Lu HY (2017) Two centuries of April-July temperature change in southeastern China and its influence on grain productivity. Science Bulletin 62(1): 40–45
27. Shi JF, Li JB, Edward R. Cook, Zhang XY, Lu HY (2012) Growth response of *Pinus tabulaeformis* to climate along an elevation gradient in the eastern Qinling Mountains, central China. Climate Research 53: 157–167
28. Shi JF, Lu HY, Wan JD, Li SF, Nie HS (2009) Winter-half year temperature reconstruction of the last century using *Pinus armandii* Franch. tree-ring width chronologies in the eastern Qinling Mountains. Quaternary Science 29: 831–836 (in Chinese)
29. Su MF, Wang HJ (2007) Relationship and its instability of ENSO-Chinese variations in droughts and wet spells. Science China- Earth Science 50:145–152 (in Chinese)
30. The compilation of China meteorological disaster Canon (2006) China meteorological disaster Canon. China Meteorological Press, Beijing (in Chinese)
31. Tian QH, Liu Y, Cai QF, Bao G, Wang WP, Xue WL, Zhu WJ, Song HM, Lei Y (2009) The Maximum Temperature of May-July Inferred from Tree-ring in Funiu Mountain since 1874 AD. Acta Geographica

Sinica 64(7): 879–887 (in Chinese)

32. Torrence C, Compo GP (1998) A practical guide to wavelet analysis. Bulletin of the American Meteorological Society 79: 61–78
33. van der Schrier G, Barichivich J, Briffa KR and Jones PD (2013) A scPDSI-based global data set of dry and wet spells for 1901–2009. Journal of Geophysical Research-Atmospheres 118, 4025–4048
34. Wigley TML, Briffa KR, Jones PD (1984) On the average value of correlated time series, with applications in dendroclimatology and hydrometeorology. Journal of Applied Meteorology and Climatology 23: 201–213
35. Wu XD (1990) Tree ring and climate change. China Meteorological Press, Beijing (in Chinese)
36. Xu HC (1993) Tree growth Chinese Pine. China Forest Industry Press, Beijing: 125–126 (in Chinese).
37. Yang L, Li JR, Peng JF, Huo JX, Chen L (2021) Temperature variation and influence mechanism of *Pinus tabulaeformis* ring width recorded since 1801 at Yao Mountain, Henan Province. Acta Ecologica Sinica 41(1):79–91
38. Yang Q, Ma ZG, Fan XG, Yang ZL, Xu ZF, Wu PL (2017) Decadal modulation of precipitation patterns over eastern China by sea surface temperature anomalies. Journal of Climate 30(17): 7017–7033
39. Zhang Y, Tian QH, Guillet S, Stoffel M (2017) 500-yr. precipitation variability in Southern Taihang Mountains, China, and its linkages to ENSO and PDO. Climatic Change 144(3): 419–432
40. Zhao YS, Shi JF, Shi SY, Ma XQ, Zhang WJ, & Wang BW, Sun XG, Lu HY, Bräuning A (2019) Early summer hydroclimatic signals are captured well by tree-ring earlywood width in the eastern Qinling mountains, central china. Climate of the Past 15(3): 1113–1131
41. Zheng QY, Shen BZ, Gong ZQ, Zhou J, Hu JG (2014) Relationship between North Pacific Oscillation in May and Drought /Flood in Summer in North China. Plateau Meteorology 3:775–785
42. Zheng YH, Shao XM, Lu F, Li Y (2016) February-may temperature reconstruction based on tree-ring widths of *Abies fargesii* from the Shennongjia area in central China. International Journal of Biometeorology 60: 1175–1181
43. Zheng YH, Zhang Y, Shao XM, Yin ZY, & Jin Z (2012) Temperature variability inferred from tree-ring widths in the Dabie mountains of subtropical central China. Trees 26(6): 1887–1894

Figures

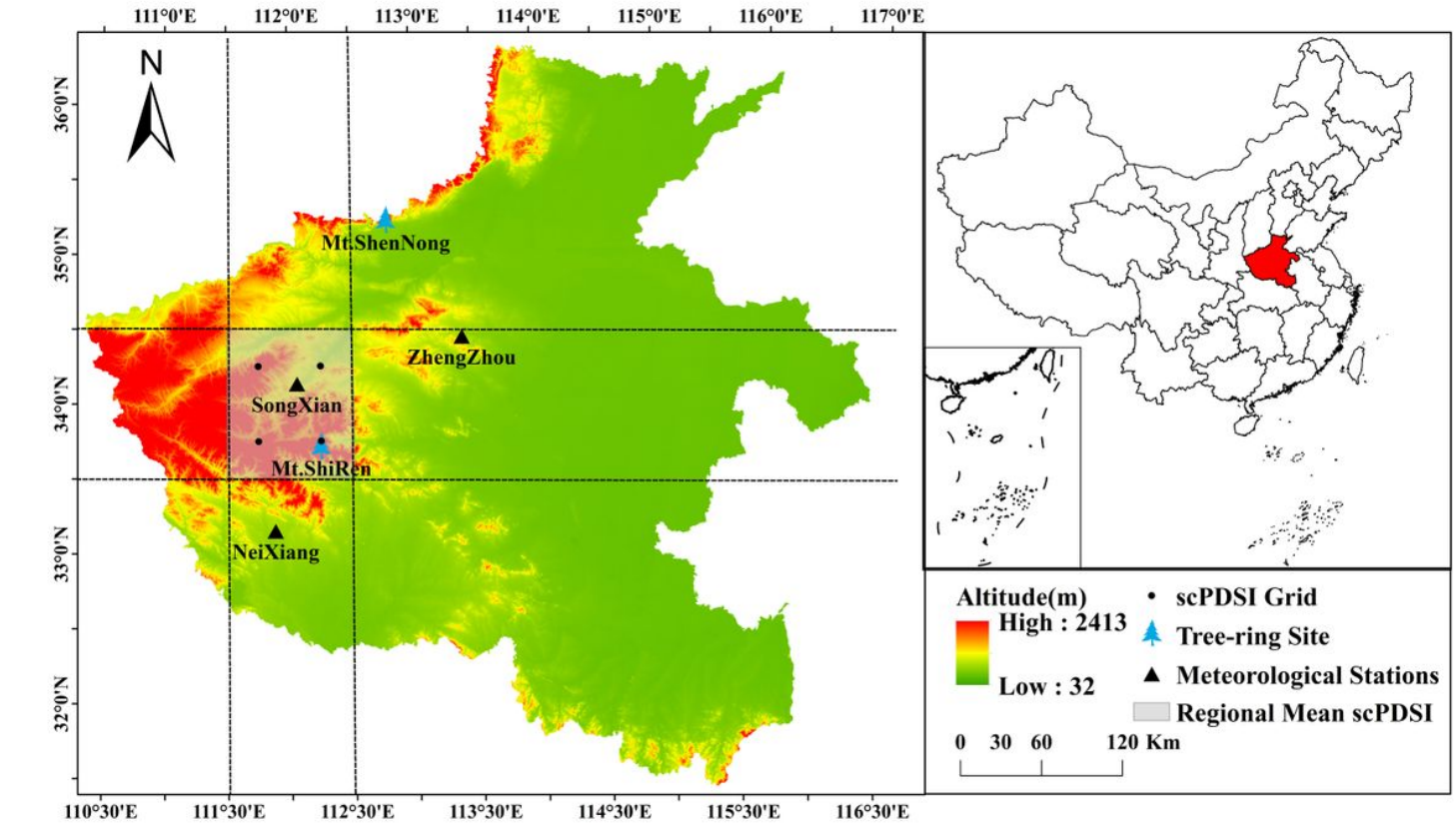

Figure 1

Map showing the study area (Mt. Shiren), Songxian and Neixiang meteorological stations, the scPDSI grid points, and regional mean value.

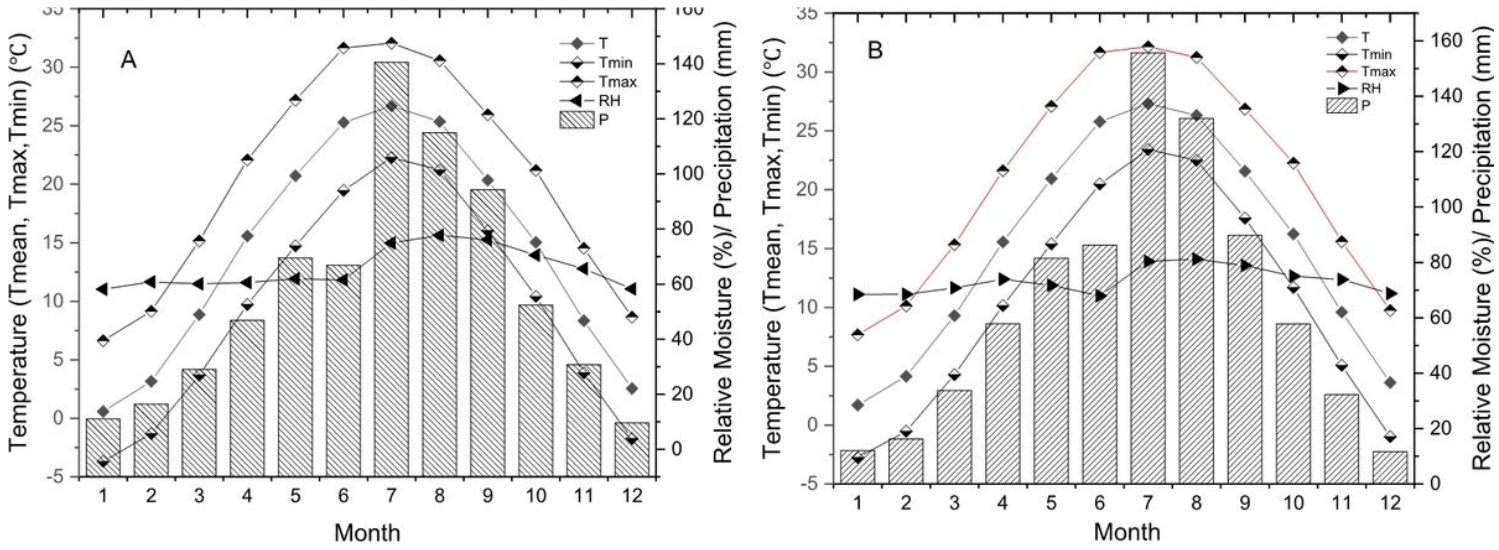

Figure 2

Tmax, T, Tmin, P and RH from Songxian (A) and Neixiang (B) meteorological stations during 1963-2016

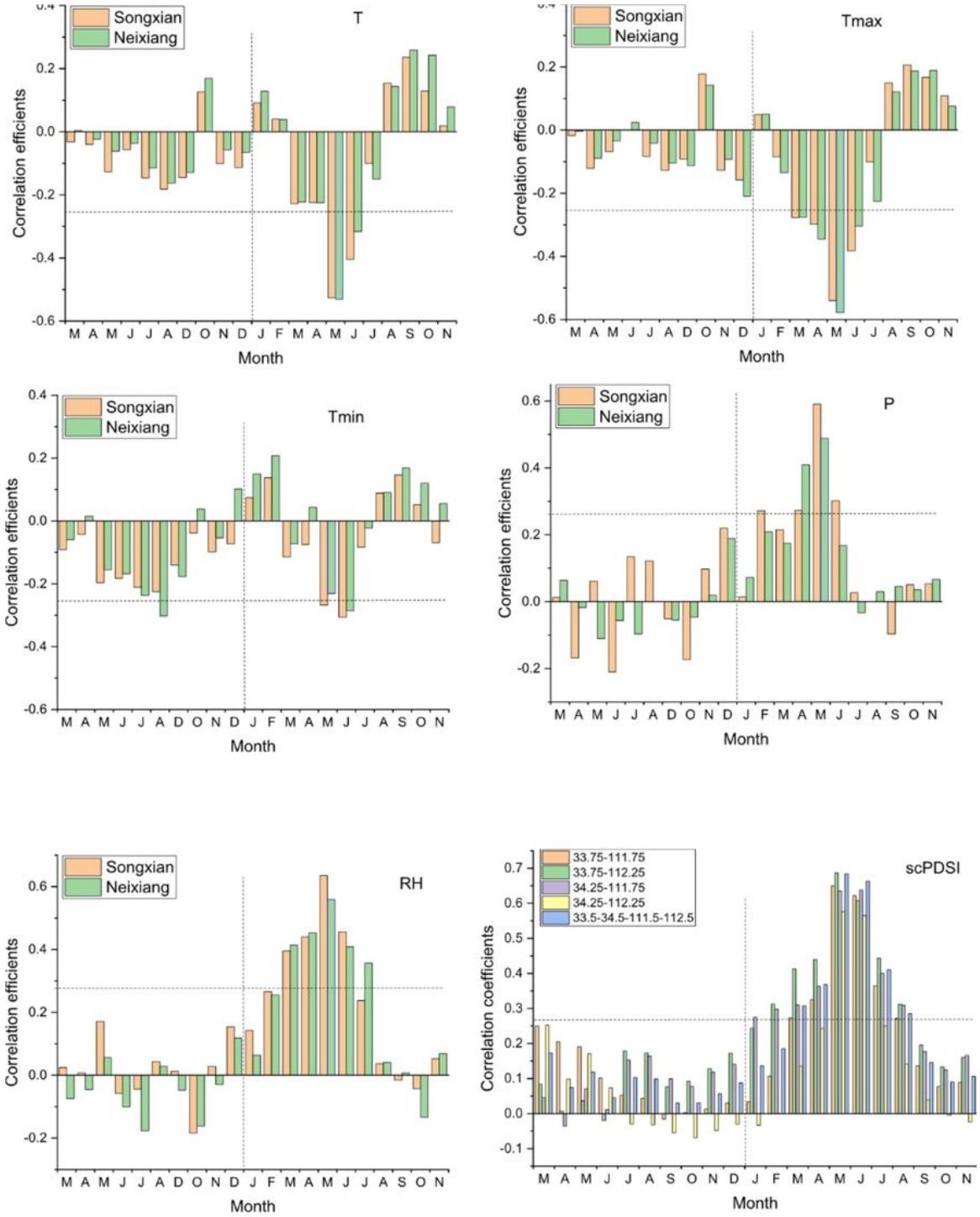

Figure 3

Correlation coefficients between the chronology and climatic factors (T, Tmax, Tmin, P, RH and scPDSI) in the Songxian (brown bar) and the Neixiang stations (green bar), respectively. The horizontal dashed line represents p< 0.05.

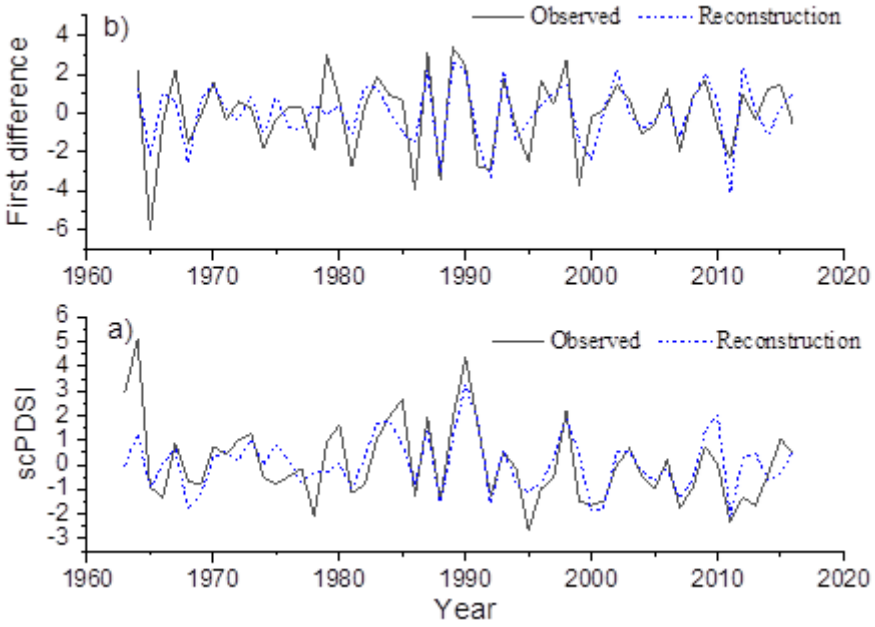

Figure 4

a) Comparison of the observed (solid line) and the reconstructed (dot line) $scPDSI_{MJ}$ during the period 1963-2016 CE at Mt. Shiren. b) Comparison of the first-order difference sequence of the observed (solid line) and reconstructed (dot line) $scPDSI_{MJ}$.

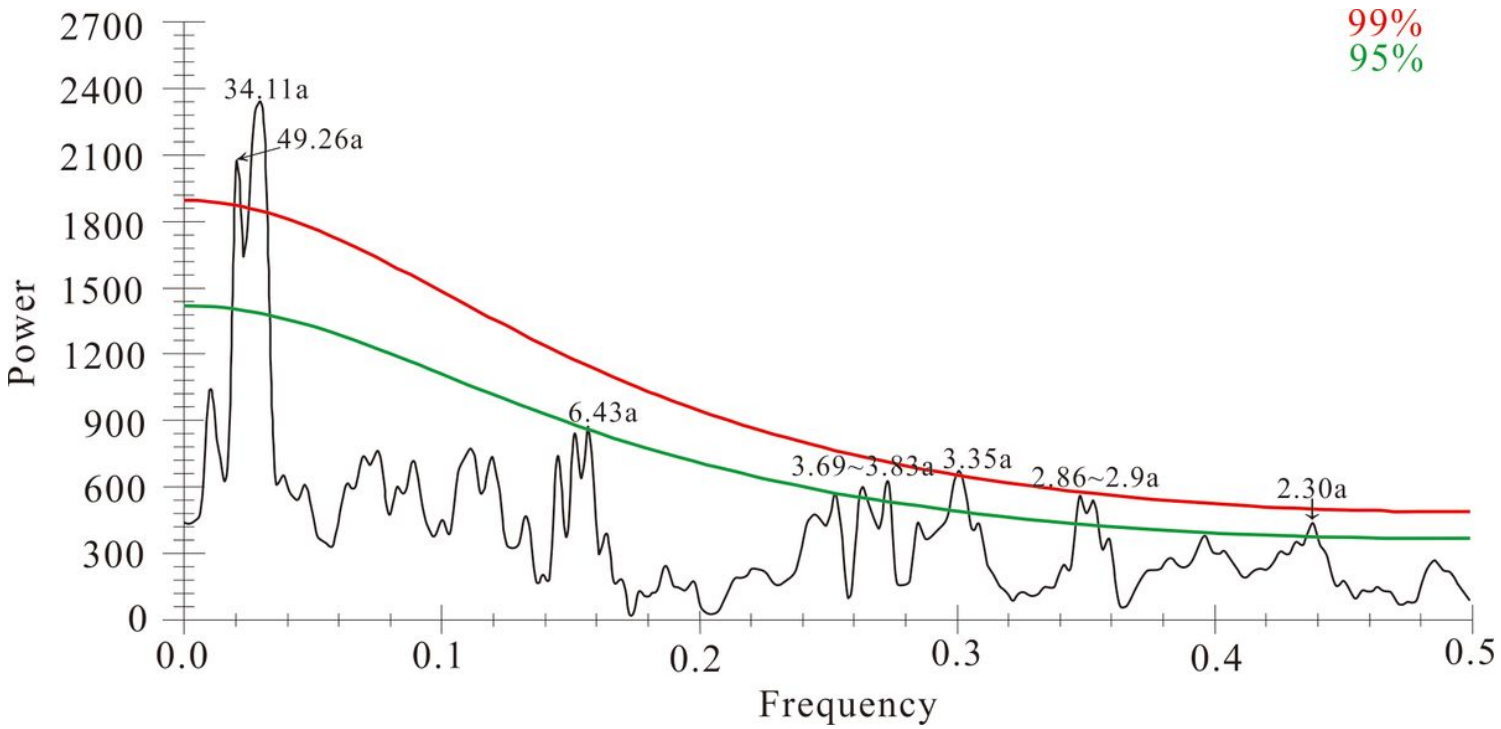

Figure 5

Results of the MTM power spectrum from reconstructed scPDSI$_{MJ}$ from 1801 to 2016 CE. The red and cyan lines indicate 99% and 95%, respectively.

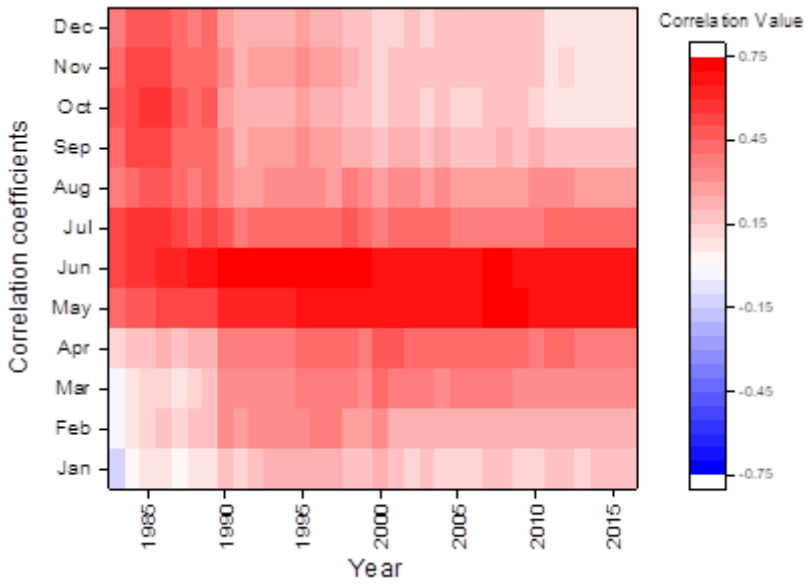

Figure 6

The moving correlation result of regional mean scPDSI$_{MJ}$

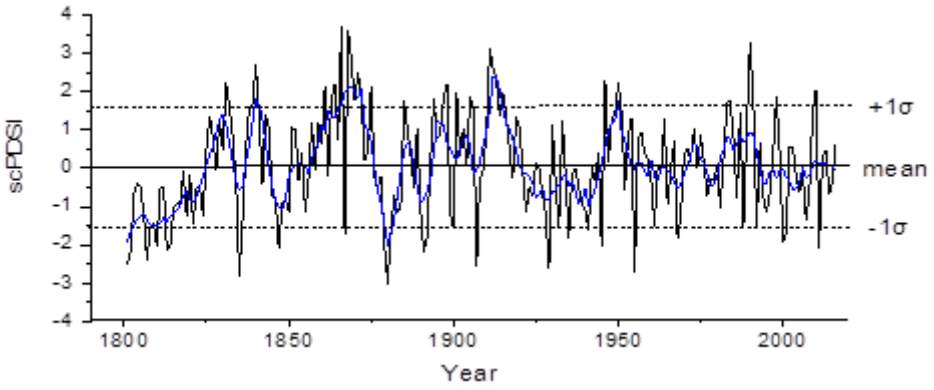

Figure 7

Reconstructed scPDSI$_{MJ}$ and 11 year smoothing curve (blue line) **at Mt. Shiren during 1801-2016.**

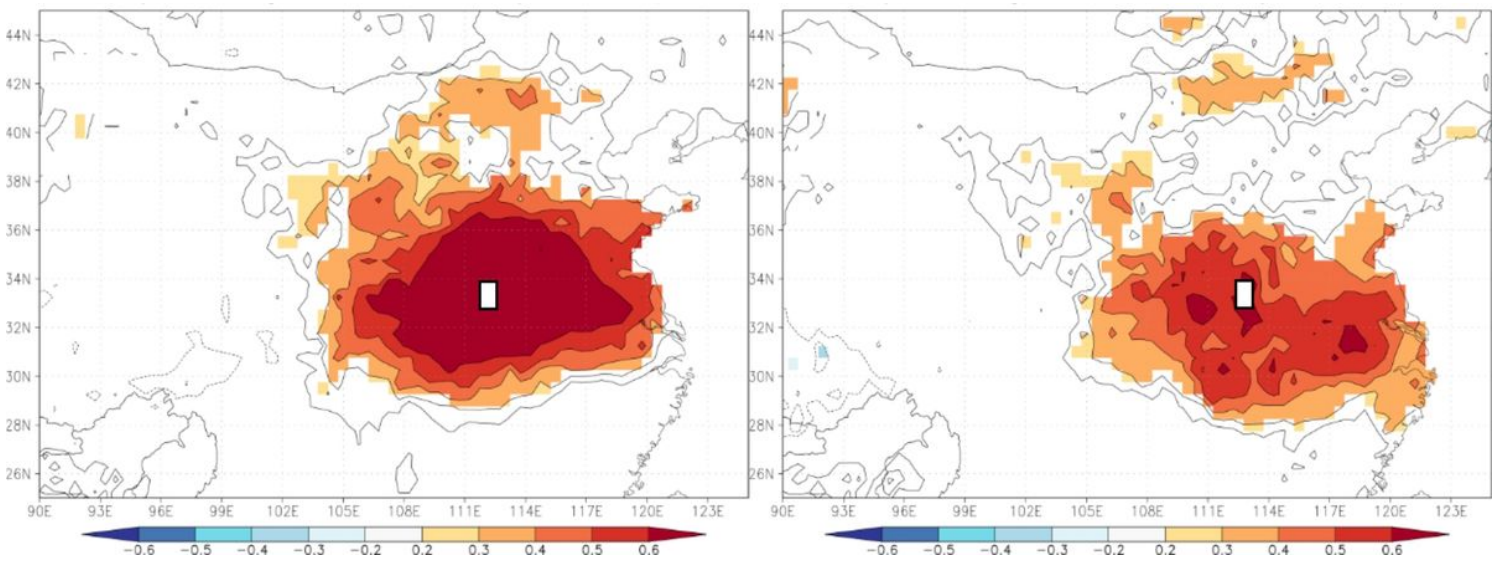

Figure 8

Spatial correlation between actual (left) and reconstructed (right) scPDSI$_{MJ}$ and scPDSI (1963-2016; 4.05early). The white rectangle represents the reconstructed scPDSI$_{MJ}$ area (33.5-34.5N, 111.5-112.5E).

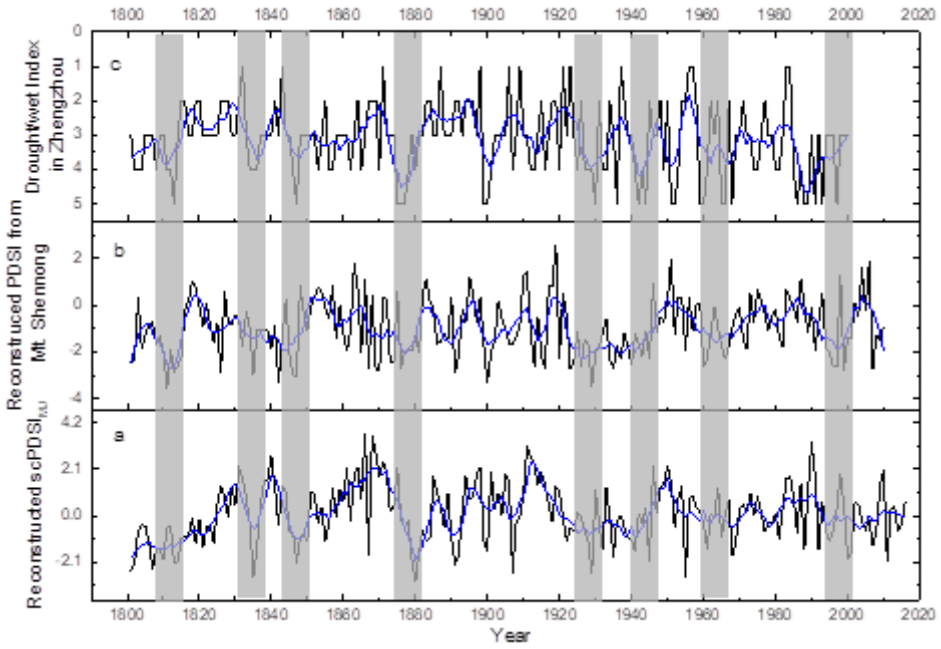

Figure 9

Comparisons of a) reconstructed regional scPDSI$_{MJ}$**, b) reconstructed PDSI from Mt. Shennong (Peng et al. 2012), and c) drought/wet index in Zhengzhou (CMA, 1981).**

The gray bars represent the same drought periods in three series.

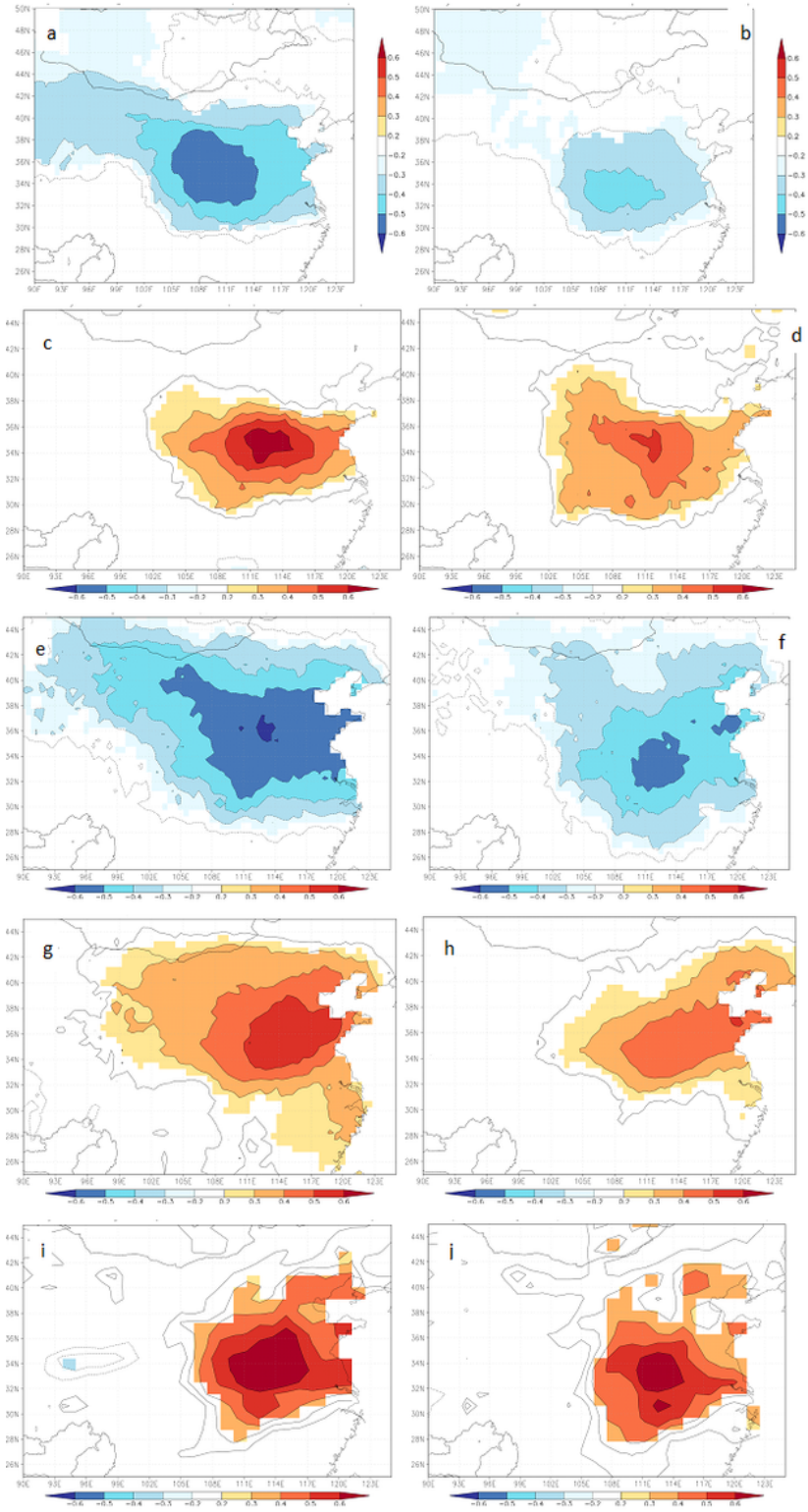

Figure 10

Spatial correlation analyses between actual (left) and reconstructed scPDSI$_{MJ}$ (right). a-b) temperature, c-d) precipitation, e-f) potential evaporation, g-h) vapor pressure (CRU TS4.04, 1963-2016), i-j) soil moisture (1979-2016, CLM/EARi, 0-10cm).

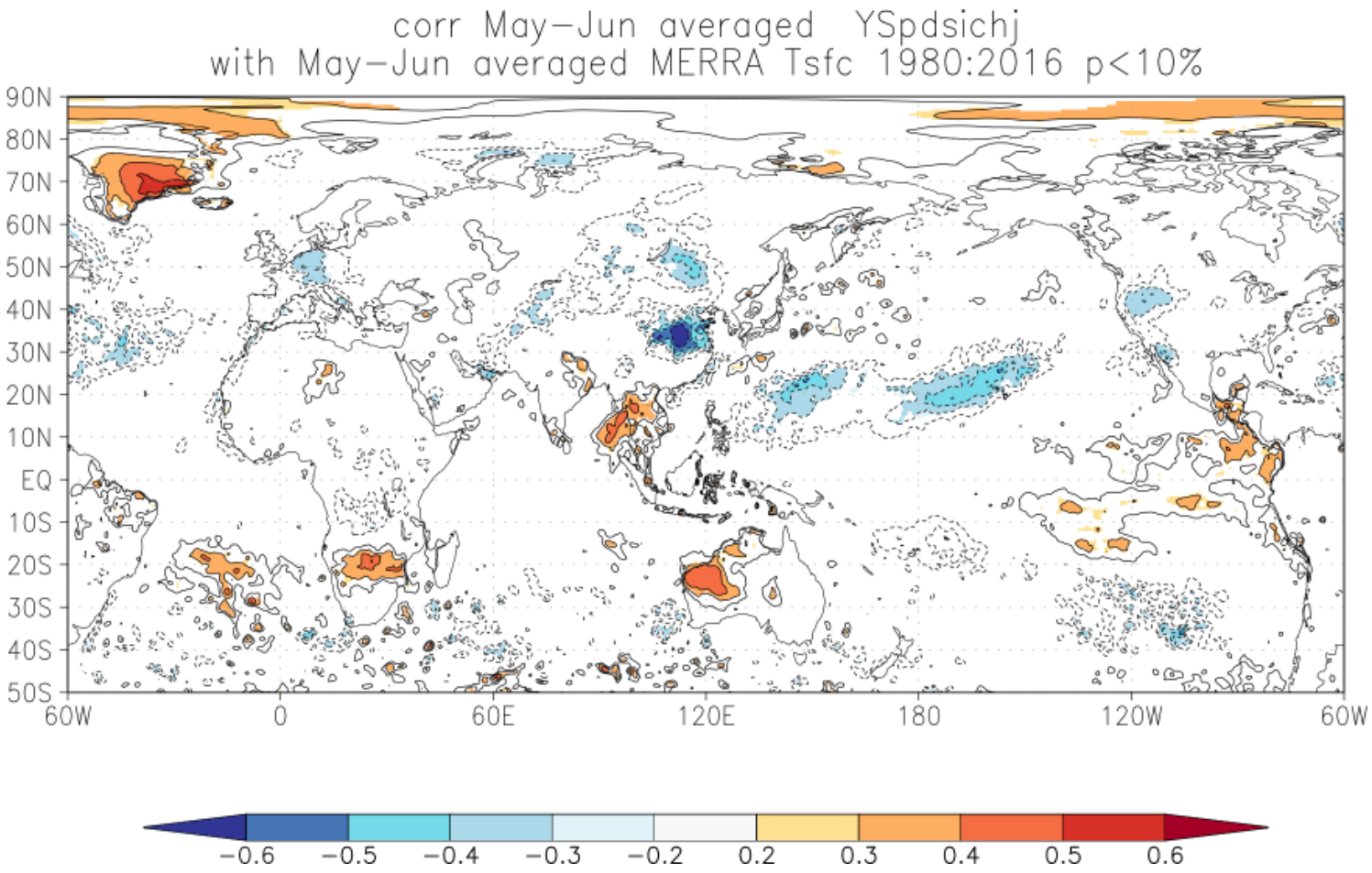

Figure 11

The relationship between tree growth and global sea surface temperature (SST, NASA MERRA-2 Tsfc, 1980-2016)